NANO LETTERS

pubs.acs.org/NanoLett

Letter

Ultrathin Layered Hyperbolic Metamaterial-Assisted Illumination Nanoscopy

Yeon Ui Lee,◆ Zhaoyu Nie,◆ Shilong Li,◆ Charles-Henri Lambert, Junxiang Zhao, Fan Yang, G. Bimananda M. Wisna, Sui Yang, Xiang Zhang, and Zhaowei Liu*

Cite This: *Nano Lett.* 2022, 22, 5916–5921

Read Online

ACCESS | Metrics & More | Article Recommendations | Supporting Information

ABSTRACT: Metamaterial-assisted illumination nanoscopy (MAIN) has been proven to be a promising approach for super-resolution microscopy with up to a 7-fold improvement in imaging resolution. Further resolution enhancement is possible in principle, however, has not yet been demonstrated due to the lack of high-quality ultrathin layered hyperbolic metamaterials (HMMs) used in the MAIN. Here, we fabricate a low-loss composite HMM consisting of high-quality bilayers of Al-doped Ag and MgO with a nominal thickness of 2.5 nm, and then use it to demonstrate an ultrathin layered hyperbolic metamaterial-assisted illumination nanoscopy (ULH-MAIN) with a 14-fold imaging resolution improvement. This improvement of resolution is achieved in fluorescent beads super-resolution experiments and verified with scanning electron microscopy. The ULH-MAIN presents a simple super-resolution imaging approach that offers distinct benefits such as low illumination power, low cost, and a broad spectrum of selectable probes, making it ideal for dynamic imaging of life science samples.

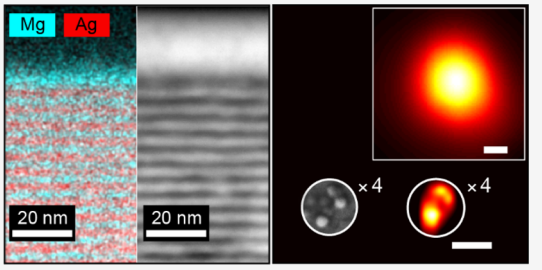

KEYWORDS: *Metamaterials, Hyperbolic metamaterials, Super-resolution microscopy, Structured illumination microscopy, Metamaterial assisted illumination, Nanoscopy*

Super-resolution fluorescence microscopies have extended our ability to explore the biological structures and dynamics below the optical diffraction limit of $\lambda/2NA$, where λ is the wavelength and NA is the numerical aperture of the objective lens.[1] Most of the super-resolution fluorescence microscopies rely on the selective excitation of fluorophores in a temporal or spatial sequence, which thus requires high intensity excitation,[2,3] sample fixation,[4] or nonlinear structured illumination.[5,6] However, these requirements impose potential risks of altering the biological structures and modifying their dynamics.[5] Such a trade-off between a minimal impact on the sample and a maximal resolution of its image eventually degrades the overall performance of these fluorophore-engineering based super-resolution microscopies.

In this context, metamaterial-assisted illumination nanoscopy (MAIN)[7−12] has been proposed to address the issue. With the MAIN, super-resolution imaging with a 7-fold resolution improvement has been demonstrated[8,9] based on the well-developed linear structured illumination strategy[13] by using hyperbolic metamaterials (HMMs) for providing a structured illumination beyond the diffraction limit. To this end, a planar HMM substrate is generally made by alternating dielectric and metal thin layers with the resultant principal components of permittivity tensor having opposite signs; as a result, surface plasmon polaritons are activated at these dielectric−metal interfaces and evanescently coupled such that structured illumination patterns carrying deep subwavelength information are creased at the top surface of the planar HMM substrate and then used for super-resolution imaging.[8,14] The imaging resolution of such a composite HMM-based MAIN is limited by the HMM's optical loss and metal layer thickness.[9,15] While ultrathin continuous metal films have recently been produced, such as copper seed Au[16] and Ag[17] thin-films and metallic quantum-well TiN thin-film,[18] their optical loss is severe at the visible frequency so that they cannot be used for MAIN. Therefore, the lack of a low-loss HMM system with ultrathin metal layers has been a major roadblock challenging the attainability of further resolution improvement of the MAIN.[19,20]

In this Letter, we demonstrate an ultrathin layered hyperbolic metamaterial assisted illumination nanoscopy (ULH-MAIN) with a 14-fold resolution improvement, enabled by a low-loss composite HMM consisting of eight 2.5 nm high-quality bilayers of Al-doped Ag and MgO. Two adjacent fluorescent beads with a center-to-center distance of 24 nm were resolved with the ULH-MAIN. In addition to such a large resolution improvement, this ULH-MAIN exhibits other

Received: May 12, 2022
Revised: July 9, 2022
Published: July 14, 2022

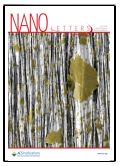

https://doi.org/10.1021/acs.nanolett.2c01932
Nano Lett. 2022, 22, 5916−5921

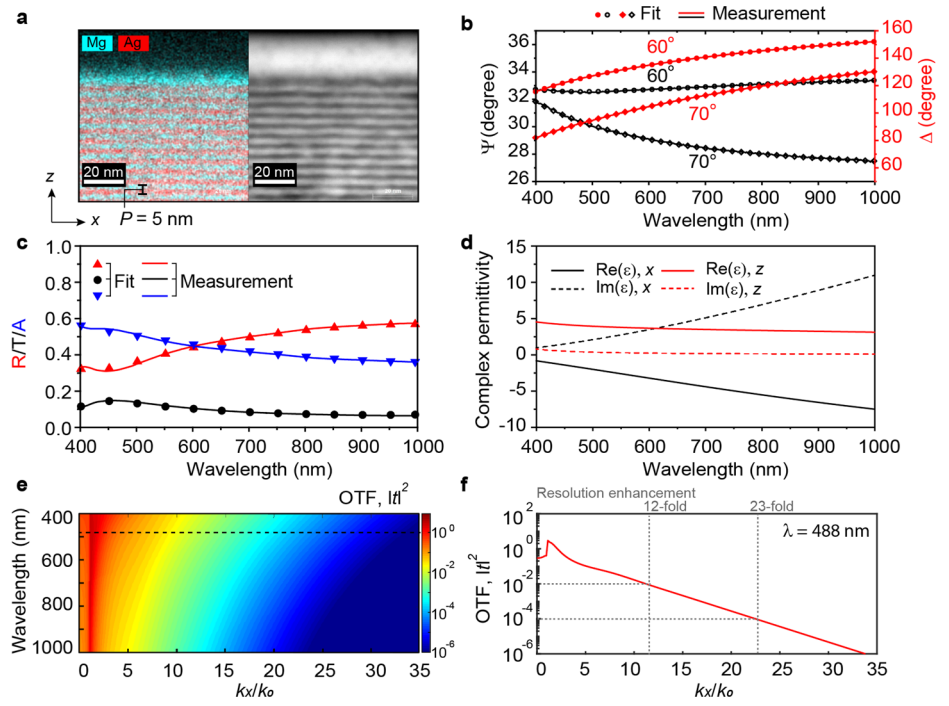

Figure 1. Ultrathin low-loss Al-doped Ag/MgO HMMs. (a) TEM images of an Al-doped Ag/MgO HMM with each individual layer having a nominal thickness of 5 nm. (b) VASE results of the HMM used in ULH-MAINs. Amplitude ratio, Ψ, and phase difference, Δ, of the reflection coefficients r_p and r_s for the p- and s-polarizations measured at 60° and 70° incidence angles are shown. The dots are the fitting results that were used to extract the permittivity tensor of the HMM. (c) Measured reflection (R), transmission (T), and absorption ($A = 1 - R - T$) spectra at normal incidence and their fitting results. (d) Extracted complex permittivity tensor. (e) Calculated OTF for the HMM with a total thickness of 45.8 nm with a nominal layer thickness of 2.5 nm. (f) Calculated OTF at λ = 488 nm.

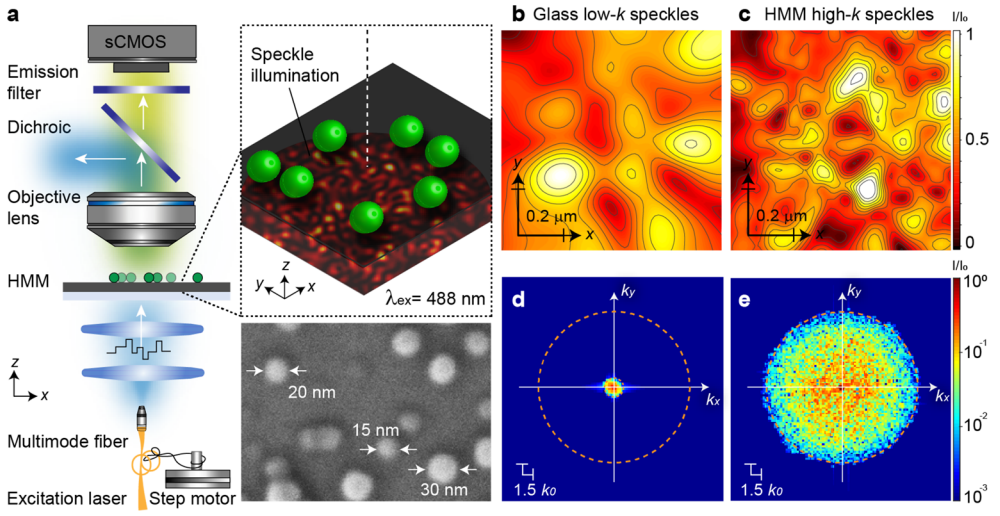

Figure 2. Principle of ULH-MAINs. (a) Schematic drawing of the setup for the ULH-MAIN consisting of a standard fluorescence microscope using an HMM substrate with a vibrating multimode fiber. The inset shows the SEM image of fluorescent beads used in the ULH-MAIN. (b,c) Intensity profiles of speckles on a glass (b) and an HMM (c), respectively, using the FDTD simulations. Randomly oriented electric dipoles with a random initial phase were used as the light source on the bottom surfaces of the glass and HMM substrates, respectively, to generate these random speckles resulting from the scattering by randomly distributed nanometer-sized defects. (d,e) Fast Fourier transforms (FFTs) of speckle patterns on the glass (d) and the HMM (e), respectively, in the spatial frequency domain.

distinct advantages such as a low excitation power, an improved photostability mediated by the HMM's inherently high Purcell factor,[21] the simplified optical setup, and a tunable spectral response for a wide range of fluorescent probes.

First, the fabrication of ultrathin low-loss HMMs used in ULH-MAINs is discussed. As a fundamental limiting factor in not only the HMMs but many other plasmonic devices, the Vollmer-Weber island growth mode[22] will be dominant when the thickness of an Ag thin film is down to the nanometer scale, forbidding the formation of a continuous ultrathin Ag film. This threshold thickness is often called the percolation threshold, and its typical value for pure Ag is around 11 nm.[19] There are several factors that might account for such a large percolation threshold, for example, the lattice mismatch, the

https://doi.org/10.1021/acs.nanolett.2c01932
Nano Lett. 2022, 22, 5916−5921

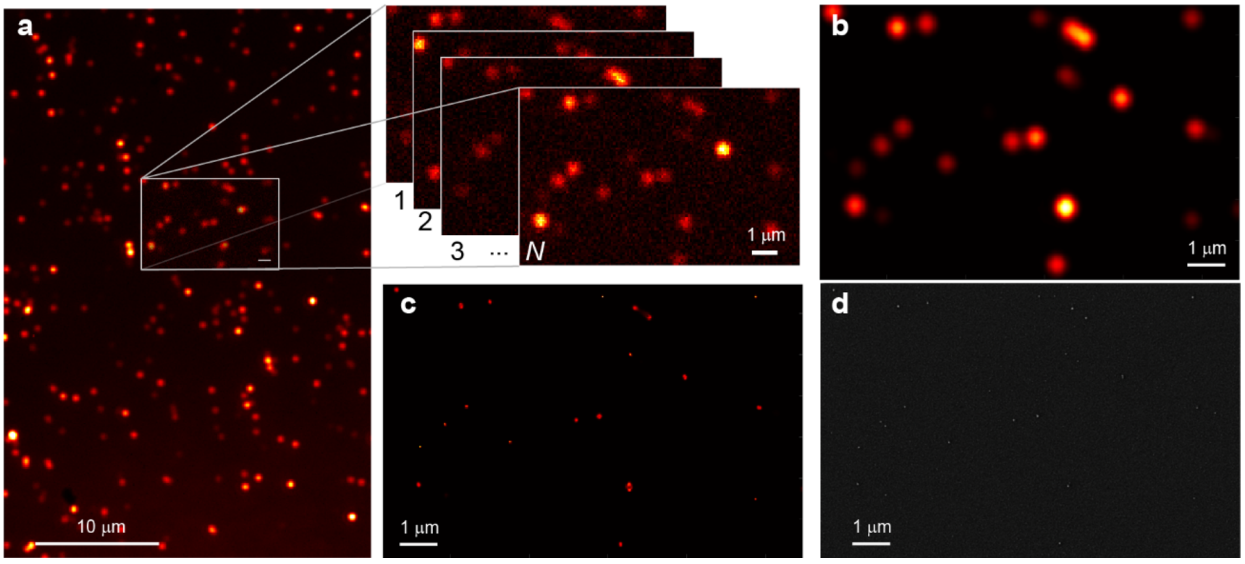

Figure 3. ULH-MAIN of single fluorescent beads. (a) Diffraction-limited image (averaged over 200 frames) of the fluorescent beads illuminated under randomly varied high-k speckles. The exposure time for each diffraction-limited image is 200 ms. A few of these frames in a small exemplary region are also shown. (b–d) Diffraction-limited image (b), ULH-MAIN super-resolution image (c), and the corresponding SEM image (d) of the fluorescent beads in this small exemplary region shown in (a).

variation in surface energy, and the difference in diffusion coefficients. Here, we have dealt with the following issues to lower the percolation threshold to a few nanometers in our ultrathin layered HMMs: (i) Al-doped Ag and MgO are picked up to minimize the lattice mismatch between these dielectric and metal layers; (ii) the addition of Al to Ag causes a slight lattice distortion but the resultant alloy film has a lower surface energy compared to the case of pure Ag, which benefits the growth of a continuous layer; and (iii) the diffusion distance of Al atoms is shorter than that of Ag atoms because the bond strength of Al–O is much larger than that of Ag–O,[23] and the diffusion distance can be further reduced by lowering the growth temperature to −150 °C and, as a result, the relatively immobile Al nuclei provide dense nucleation sites for early, continuous film formation. Figure 1a shows the typical transmission electron microscopy (TEM) images of the fabricated HMMs (Methods), where the ultrathin continuous metal films well below the 11 nm percolation threshold of pure Ag are clearly visible.

The optical constant of the HMM used in ULH-MAINs was obtained from variable angle spectroscopic ellipsometry (VASE) and cross-checked with the measured reflection, transmission, and absorption results, as summarized in Figure 1b–d (Methods). As can be clearly seen from Figure 1d, there is an opposite sign for the in-plane and out-of-plane components of the permittivity tensor, that is, a type II hyperbolic dispersion (see the effect of unit cell periodicity on the dispersion in Supporting Information S1). The optical transfer function (OTF) can then be calculated using the experimentally extracted anisotropic permittivity tensor, and the result is plotted in Figure 1e,f (see the effect of unit cell periodicities on the OTF in Supporting Information S2). It shows a record high cutoff spatial-frequency $k_{cutoff} = 12k_0$ (k_0 is the spatial frequency in vacuum) at $\lambda = 488$ nm when $OTF_{cutoff} = 0.01$, which allows a maximum imaging resolution around 20 nm. Such a record high k_{cutoff} is enabled by not only the nanometer scale layer thickness of the HMM but also its low optical loss. It is worth noting that although the imaginary part of the in-plane permittivity component of the HMM is slightly larger than that of bulk Ag due to the imperfect interfaces, the HMM's optical loss is still relatively low because pure Ag at this thickness will not be a continuous film.

The fabricated HMMs with the record high k_{cutoff} are then used for MAIN, leading to the ULH-MAIN. The implementation of the ULH-MAIN is simple and straightforward by using a standard fluorescence microscope with speckle illumination, as shown in Figure 2a. The speckle illumination was initialized by coupling a 488 nm excitation laser through a vibrating multimode fiber to the backside of the HMM. After passing through the HMM, the excitation laser speckles (~10 W/cm^2) were further scrambled and squeezed into the hyperbolic modes via randomly scattering at the nanometer-scale superlattice defects of the HMM film (see the surface and interface roughness measurements in Supporting Information S3). Note that such a Rayleigh scattering is efficient in the HMM due to the inherently high Purcell factor of these hyperbolic modes.[21] Random speckle patterns were finally generated on top of the HMM, as shown in Figure 2b–e, which contain high spatial frequencies up to $12k_0$, that is, 1 order of magnitude higher than that on top of a glass. Emission of fluorescent beads on top of the HMM substrate excited by these high-k speckles was collected by a 100×/1.49 NA objective lens and then imaged with an sCMOS camera, forming a diffraction-limited fluorescence image. Two hundred such diffraction-limited images of the fluorescent beads illuminated with 200 randomly varied high-k speckles, done by mechanically vibrating the multimode fiber using a step motor, were recorded and processed with the blind-SIM algorithm,[8] such that a super-resolution image of the beads was eventually reconstructed, as will be discussed in detail below. It is worth noting that there is a 10 nm MgO protection layer deposited on top of the HMM to protect Ag from oxidation and reduce the quenching effect of fluorescent beads.

The ULH-MAIN super-resolution imaging of single fluorescent beads with an average diameter of 50 nm is summarized in Figure 3. Figure 3a shows the diffraction-

https://doi.org/10.1021/acs.nanolett.2c01932
Nano Lett. 2022, 22, 5916–5921

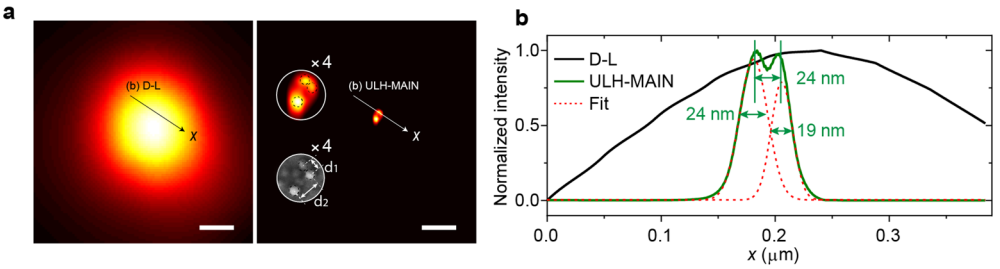

Figure 4. ULH-MAIN of adjacent fluorescent beads. (a) Diffraction-limited (D-L) image (left panel), ULH-MAIN super-resolution image (right panel), and the corresponding SEM image (inset) of few adjacent fluorescent beads. The scale bars are 200 nm. A 4× magnified view of the ULH-MAIN image and the corresponding SEM image view are shown in the circular insets, where the center-to-center distances of two adjacent beads are d_1 = 24 nm and d_2 = 52 nm. (b) Intensity profiles along the lines shown in (a). Compared with the D-L image, ULH-MAIN image shows a clear separation of two adjacent beads with the distance d_1. The center-to-center distance of the adjacent beads is obtained by fitting the super-resolution line with two Gaussian line shapes.

limited image which is the intensity average of 200 different diffraction-limited image frames obtained under randomly varied high-k speckle illuminations (a zoom in view is shown in Figure 3b). The high-k information implicitly imprinted in these diffraction-limited image frames was extracted with the blind-SIM algorithm,[8] and the resultant reconstructed super-resolution image in a small exemplary region (i.e., Figure 3b) is shown in Figure 3c where single 50 nm beads are clearly resolved. To validate such a super-resolution ability of the ULH-MAIN, scanning electron microscope (SEM) imaging of these beads in the small exemplary region was carried out by gently removing the cover glass when the sample was dried, and the result is given in Figure 3d. As can be seen, the ULH-MAIN has indeed successfully revealed the location of the fluorescent beads and their size.

To further clarify the resolution of the ULH-MAIN, super-resolution imaging of adjacent fluorescent beads was implemented, and the results are summarized in Figure 4. A minimum center-to-center distance of 24 nm of two adjacent fluorescent beads was resolved and verified with the SEM. The obtained resolution is the result of the high-k speckles with the k_{cutoff} of $12k_0$ (corresponding to a spatial correlation length down to 20 nm) supported by the fabricated ultrathin low-loss HMM. According to the theory of super-resolution fluorescence imaging with structured illumination,[13] the resolution enhancement is $1 + k_{cutoff}/k_0$ at the emission (detection) wavelength; therefore, the k_{cutoff} of $12k_0$ at the excitation wavelength results in a resolution enhancement around 13 at the emission wavelength. It is worth noting that such a great improvement of the resolution can only be achieved within the optical near fields where the electric field intensity decreases exponentially with distance from the HMM substrate; as a result, the ULH-HMM demonstrated here is a powerful near-field imaging technique with a depth limitation, as discussed in our previous studies.[8,9]

In conclusion, we developed low-loss ultrathin Al-doped Ag and MgO layered hyperbolic metamaterials for generating hyperfine speckle illumination. Al-doped Ag thin films (2.5 nm thick) were successively fabricated by minimizing the lattice mismatch and reducing the diffusion distance. An ultrathin layered hyperbolic metamaterial-assisted illumination nanoscopy, termed ULH-MAIN, with a record high 14-fold resolution improvement was demonstrated. This ULH-MAIN could be beneficial for various imaging and metrology applications, where far-field super-resolution imaging would be required. Since super-resolution imaging of a life sample with MAIN has been demonstrated in our previous work, bioimaging with ULH-MAIN is straightforward in the future with appropriate selection of biosamples in order to fully utilize the ∼20 nm resolution of the ULH-MAIN. Although this resolution is still lower than that of conventional SEM (not to mention the cryogenic SEM), the possibility of live-cell imaging makes the ULH-MAIN an attractive noninvasive bioimaging option.

METHODS

Device Fabrication. The Al-doped Ag/MgO multilayers (eight pairs) were grown by magnetron sputtering on a glass coverslip. The cosputtering rate for Al and Ag is 0.3 Å/s and the deposition rate of MgO is 0.05 Å/s. The deposition was performed at the temperature of −150 °C. There is a 10 nm MgO protection layer deposited on top of the HMM multilayer to protect Ag from oxidation. Fluorescent beads were drop-cast onto this HMM substrate in the end.

Complex Permittivity Measurement. A rotating polarizer-type spectroscopic ellipsometer (J.A. Woollam M-2000D) was used to characterize the fabricated HMM multilayers and the data were processed with CompleteEASE software. Measurements were performed in the reflection mode over a 300−1000 nm spectral range for 60° and 70° incidence angles. The measured ellipsometric parameters Ψ and $\Delta$are defined as the amplitude ratio and the phase difference of the reflection coefficients r_p and r_s for the p- and s-polarizations, respectively, via the relation $r_p/r_s = \tan(\Psi)\cdot\exp(i(\delta_p - \delta_s))$, where δ is the phase. Figure 1b shows the amplitude ratio Ψ and the phase difference Δ measured by the spectroscopic ellipsometry (SE) data at 60° and 70° incidence angles. These HMM multilayers are treated as a uniaxial layer. Note that the effective medium approximation (EMA) is widely used in the theoretical model to obtain an effective permittivity of alternating multilayers from permittivities of the respective bulk metals and dielectrics of a composite HMM; however, it is no longer accurate for the ultrathin metal layered HMM used in this work due to the nonlocal or quantum size effect in the ultrathin metals.[9,18,24] The permittivity of the ultrathin layered HMMs was obtained by performing ellipsometry measurement of the entire multilayers, instead of using EMA, which requires the permittivity of each layer. By applying the transfer matrix method with the SE measurement data, a good agreement between the measured reflection R, transmission T, and absorption $A = 1-R-T$ spectra and the calculated spectra is obtained (Figure 1c). Figure 1d shows the extracted complex permittivity.

https://doi.org/10.1021/acs.nanolett.2c01932
Nano Lett. 2022, 22, 5916−5921

■ ASSOCIATED CONTENT

Supporting Information

The Supporting Information is available free of charge at https://pubs.acs.org/doi/10.1021/acs.nanolett.2c01932.

(Section S1) unit cell periodicity effect on HMM dispersion; (Section S2) experimental demonstration of OTF versus HMM period; (Section S3) surface and interface roughness measurement (PDF)

■ AUTHOR INFORMATION

Corresponding Author

Zhaowei Liu − *Department of Electrical and Computer Engineering, University of California, San Diego, La Jolla, California 92093, United States; Materials Science and Engineering Program, University of California, San Diego, La Jolla, California 92093, United States;* orcid.org/0000-0002-5732-8109; Email: zhaowei@ucsd.edu

Authors

Yeon Ui Lee − *Department of Electrical and Computer Engineering, University of California, San Diego, La Jolla, California 92093, United States; Department of Physics, Chungbuk National University, Cheongju, Chungbuk 28644, South Korea;* orcid.org/0000-0001-8857-1251

Zhaoyu Nie − *Department of Mechanical Engineering, University of California, Berkeley, California 94720, United States*

Shilong Li − *Department of Electrical and Computer Engineering, University of California, San Diego, La Jolla, California 92093, United States; Light-Matter Interactions for Quantum Technologies Unit, Okinawa Institute of Science and Technology Graduate University, Onna, Okinawa 904-0495, Japan*

Charles-Henri Lambert − *Department of Materials, ETH Zürich, CH-8093 Zürich, Switzerland*

Junxiang Zhao − *Department of Electrical and Computer Engineering, University of California, San Diego, La Jolla, California 92093, United States*

Fan Yang − *Department of Electrical and Computer Engineering, University of California, San Diego, La Jolla, California 92093, United States*

G. Bimananda M. Wisna − *Materials Science and Engineering Program, University of California, San Diego, La Jolla, California 92093, United States*

Sui Yang − *Department of Mechanical Engineering, University of California, Berkeley, California 94720, United States; Materials Science and Engineering, School for Engineering of Matter Transport and Energy, Arizona State University, Tempe, Arizona 85287, United States*

Xiang Zhang − *Faculty of Science and Engineering, The University of Hong Kong, Hong Kong, Hong Kong, China*

Complete contact information is available at: https://pubs.acs.org/10.1021/acs.nanolett.2c01932

Author Contributions

◆Y.U.L., Z.N., and S.L. contributed equally to this work.

Author Contributions

Y.U.L., Z.N., S.L., and Z.L. conceived and designed the experiment. Y.U.L., Z.N., S.L., C.H.L., J.Z., F.Y., G.B.M.W. performed the experiments. Y.U.L., Z.N., S.L. wrote the manuscript which was revised by all authors.

Notes

The authors declare no competing financial interest.

■ ACKNOWLEDGMENTS

This work was supported by the Gordon and Betty Moore Foundation (to Z.L.). Y.U.L. acknowledges NRF Grant (2014M3A6B3063708, 2021R1F1A1062916).

■ REFERENCES

(1) Abbe, E. *Arch. für mikroskopische Anat.* **1873**, *9*, 413−468.

(2) Hein, B.; Willig, K. I.; Hell, S. W. Stimulated Emission Depletion (STED) Nanoscopy of a Fluorescent Protein-Labeled Organelle inside a Living Cell. *Proc. Natl. Acad. Sci. U. S. A.* **2008**, *105* (38), 14271−14276.

(3) Grotjohann, T.; Testa, I.; Reuss, M.; Brakemann, T.; Eggeling, C.; Hell, S. W.; Jakobs, S. RsEGFP2 Enables Fast RESOLFT Nanoscopy of Living Cells. *Elife* **2012**, *2012* (1), 1−14.

(4) Shroff, H.; Galbraith, C. G.; Galbraith, J. A.; Betzig, E. Live-Cell Photoactivated Localization Microscopy of Nanoscale Adhesion Dynamics. *Nat. Methods* **2008**, *5* (5), 417−423.

(5) Li, D.; Shao, L.; Chen, B.-C.; Zhang, X.; Zhang, M.; Moses, B.; Milkie, D. E.; Beach, J. R.; Hammer, J. A.; Pasham, M.; Kirchhausen, T.; Baird, M. A.; Davidson, M. W.; Xu, P.; Betzig, E. Extended-Resolution Structured Illumination Imaging of Endocytic and Cytoskeletal Dynamics. *Science* **2015**, *349* (6251), aab3500.

(6) Gustafsson, M. G. L. Nonlinear Structured-Illumination Microscopy: Wide-Field Fluorescence Imaging with Theoretically Unlimited Resolution. *Proc. Natl. Acad. Sci. U. S. A.* **2005**, *102* (37), 13081−13086.

(7) Ma, Q.; Liu, Z. Metamaterial-Assisted Illumination Nanoscopy. *Natl. Sci. Rev.* **2018**, *5* (2), 141−143.

(8) Lee, Y. U.; Zhao, J.; Ma, Q.; Khorashad, L. K.; Posner, C.; Li, G.; Wisna, G. B. M.; Burns, Z.; Zhang, J.; Liu, Z. Metamaterial Assisted Illumination Nanoscopy via Random Super-Resolution Speckles. *Nat. Commun.* **2021**, *12* (1), 1559.

(9) Lee, Y. U.; Posner, C.; Nie, Z.; Zhao, J.; Li, S.; Bopp, S. E.; Wisna, G. B. M.; Ha, J.; Song, C.; Zhang, J.; Yang, S.; Zhang, X.; Liu, Z. Organic Hyperbolic Material Assisted Illumination Nanoscopy. *Adv. Sci.* **2021**, *8* (22), 2102230.

(10) Bezryadina, A.; Zhao, J.; Xia, Y.; Zhang, X.; Liu, Z. High Spatiotemporal Resolution Imaging with Localized Plasmonic Structured Illumination Microscopy. *ACS Nano* **2018**, *12* (8), 8248−8254.

(11) Ponsetto, J. L.; Bezryadina, A.; Wei, F.; Onishi, K.; Shen, H.; Huang, E.; Ferrari, L.; Ma, Q.; Zou, Y.; Liu, Z. Experimental Demonstration of Localized Plasmonic Structured Illumination Microscopy. *ACS Nano* **2017**, *11* (6), 5344−5350.

(12) Narimanov, E. Hyperstructured Illumination. *ACS Photonics* **2016**, *3* (6), 1090−1094.

(13) Ströhl, F.; Kaminski, C. F. Frontiers in Structured Illumination Microscopy. *Optica* **2016**, *3* (6), 667.

(14) Liu, Z.; Lee, H.; Xiong, Y.; Sun, C.; Zhang, X. Far-Field Optical Hyperlens Magnifying Sub-Diffraction-Limited Objects. *Science* **2007**, *315* (5819), 1686−1686.

(15) Smith, D. R.; Schurig, D. Electromagnetic Wave Propagation in Media with Indefinite Permittivity and Permeability Tensors. *Phys. Rev. Lett.* **2003**, *90* (7), 4.

(16) Maniyara, R. A.; Rodrigo, D.; Yu, R.; Canet-Ferrer, J.; Ghosh, D. S.; Yongsunthon, R.; Baker, D. E.; Rezikyan, A.; García de Abajo, F. J.; Pruneri, V. Tunable Plasmons in Ultrathin Metal Films. *Nat. Photonics* **2019**, *13* (5), 328−333.

(17) Formica, N.; Ghosh, D. S.; Carrilero, A.; Chen, T. L.; Simpson, R. E.; Pruneri, V. Ultrastable and Atomically Smooth Ultrathin Silver Films Grown on a Copper Seed Layer. *ACS Appl. Mater. Interfaces* **2013**, *5* (8), 3048−3053.

(18) Qian, H.; Li, S.; Li, Y.; Chen, C.-F.; Chen, W.; Bopp, S. E.; Lee, Y.-U.; Xiong, W.; Liu, Z. Nanoscale Optical Pulse Limiter Enabled by Refractory Metallic Quantum Wells. *Sci. Adv.* **2020**, *6* (20), 1−7.

(19) Chen, W.; Thoreson, M. D.; Ishii, S.; Kildishev, A. V.; Shalaev, V. M. Ultra-Thin Ultra-Smooth and Low-Loss Silver Films on a Germanium Wetting Layer. *Opt. Express* **2010**, *18* (5), 5124.
(20) Zhukovsky, S. V.; Kidwai, O.; Sipe, J. E. Physical Nature of Volume Plasmon Polaritons in Hyperbolic Metamaterials. *Opt. Express* **2013**, *21* (12), 14982.
(21) Lee, Y. U.; Li, S.; Bopp, S. E.; Zhao, J.; Nie, Z.; Posner, C.; Yang, S.; Zhang, X.; Zhang, J.; Liu, Z. Unprecedented Fluorophore Photostability Enabled by Low-Loss Organic Hyperbolic Materials. *Adv. Mater.* **2021**, *33* (9), 2006496.
(22) Luth, H. *Solid Surfaces Interfaces and Thin Film*; Springer, New York, 2001.
(23) Gu, D.; Zhang, C.; Wu, Y. K.; Guo, L. J. Ultrasmooth and Thermally Stable Silver-Based Thin Films with Subnanometer Roughness by Aluminum Doping. *ACS Nano* **2014**, *8* (10), 10343−10351.
(24) Tumkur, T.; Barnakov, Y.; Kee, S. T.; Noginov, M. A.; Liberman, V. Permittivity Evaluation of Multilayered Hyperbolic Metamaterials: Ellipsometry vs. Reflectometry. *J. Appl. Phys.* **2015**, *117* (10), 103104.

https://doi.org/10.1021/acs.nanolett.2c01932
Nano Lett. 2022, 22, 5916−5921